Available online at www.sciencedirect.com
ScienceDirect
Journal of Magnetic Resonance 192 (2008) 8–16
JMR Journal of Magnetic Resonance
www.elsevier.com/locate/jmr

Through-space MP-CPMAS experiments between spin-1/2 and half-integer quadrupolar nuclei in solid-state NMR

B. Hu, J.P. Amoureux *, J. Trébosc, S. Hafner

UCCS, CNRS-8181, Lille University, Fr-59652 Villeneuve d'Ascq, France

Received 25 October 2007; revised 11 January 2008
Available online 30 January 2008

Abstract

We present a new CPMAS method that allows the acquisition of through-space 2D HETCOR spectra between spin-1/2 nuclei and half-integer quadrupolar nuclei in the solid state. It uses rotor-synchronized selective pulses on the quadrupolar nucleus and continuous-wave RF irradiation on the spin-1/2 nucleus to create hetero-nuclear dipolar coherences. The method is more robust, more efficient, and easier to set up than the standard CPMAS transfer.

Keywords: Solid-state NMR; Quadrupolar nuclei; HETCOR; Dipolar coupling

1. Introduction

Cross-polarization (CP) [1,2] has played an instrumental role in extending the analytical capabilities of solid-state nuclear magnetic resonance (NMR) to the studies of what were once considered 'difficult' nuclei, such as ^{13}C, ^{15}N, and ^{29}Si. Nuclear polarization is usually transferred from abundant spins I with large gyromagnetic ratio γ_I and short longitudinal relaxation time T_{1I} to diluted spins S with small γ_S or long T_{1S}, in order to increase the magnetization of S and the repetition rate of the experiment. For resolution enhancement, this transfer is usually combined with magic-angle spinning (MAS) [3]. The use of CPMAS method is not limited to signal enhancement, but can be extended to include spectral editing and various two-dimensional (2D) techniques, such as hetero-nuclear correlation (HETCOR) experiments. These experiments can provide detailed information about complex structures in chemistry, biology and materials science by identifying atoms in local 'proximity' to one another. For spin-1/2 nuclei, HETCOR methods have become well established for such structural investigations using CPMAS [4,5]. Improvements of CW-CPMAS (Continuous-Wave CPMAS) for spins 1/2 have also been developed, giving many different sequences such as RAMP CP [6], SPICP [7], D-AMCP [8], or S-AMCP [9,10], in order to broaden Hartmann–Hahn conditions, but these improvements have never been applied to quadrupolar systems. Indeed, these methods were designed for radio frequency (RF) fields much larger than the spinning speed. Moreover, applying original CW-CPMAS to half-integer quadrupolar nuclei (spin: 3/2, 5/2, 7/2, 9/2) represents additional challenges compared to spins 1/2 due to the complex spin dynamics during spin-locking of these nuclei and during the polarization transfer period. In powdered samples, CP dynamics is strongly anisotropic with respect to crystallite orientation and depends on numerous experimental parameters [11,12]. As a result, in most cases, CW-CPMAS involving quadrupolar nuclei is much less sensitive than the transfer between two spin-1/2 nuclei, especially when two different quadrupolar nuclei are involved [13,14]. To be efficient, the RF-fields must then be very weak, which leads to a large sensitivity to off-resonance irradiation. This is the reason why CW-CPMAS HETCOR spectra of quadrupolar systems are often recorded by superimposing several com-

* Corresponding author. Fax: +33 2 20 43 68 14.
E-mail address: jean-paul.amoureux@univ-lillel.fr (J.P. Amoureux).

1090-7807/$ - see front matter © 2008 Elsevier Inc. All rights reserved.
doi:10.1016/j.jmr.2008.01.008

plementary experiments performed with different offsets, especially at high magnetic field [15]. Moreover, the RF matching curves show numerous dips related to level crossings [16] or rotary resonance phenomenon [17], which means that setting up the CW-CPMAS transfer is not easy, especially with samples of low sensitivity. Also, the efficiency of the transfer decreases significantly with increasing second-order quadrupole interactions [16], and hence the sites with large quadrupolar constant values ($C_Q = e^2qQ$) are often hardly observable. As a result, methods based on CW-CPMAS transfer to or from half-integer quadrupolar nuclei are subject to many important experimental and theoretical limitations and are thus not commonly used.

Recently a sequence, named MP-CPMAS (Multiple-pulse CPMAS) has been presented [18]. It is composed of a CW irradiation on one channel and rotor-synchronized pulses on the other channel. The sequence was originally designed to reduce ^{1}H RF power in ^{1}H–^{13}C CP at ultra-fast MAS speed. The authors made a comparison on alanine under $\nu_R = 60$ kHz MAS between CW-CPMAS with proton RF amplitude of $\nu_{1H} = 4$ kHz and MP-CPMAS using short and strong pulses (0.35 μs and $\nu_{1H} = 280$ kHz) leading to the same averaged 4 kHz RF-field on ^{1}H. In both cases, the ^{13}C RF-field (ν_{1C}) was close to either ν_R or $2\nu_R$. The signal to noise ratio under MP-CPMAS conditions was approximately 50% larger than that obtained with a CW-CPMAS experiment performed with either low (4 kHz) or high (100 kHz ramped) ^{1}H power. As it utilizes a weak average RF-field, this method is close to that used for quadrupolar nuclei where RF-field is most of the time smaller than ν_R. In this article, we adapt the MP-CPMAS method to avoid the previously described limitations observed with CW-CPMAS transfers between spin-1/2 and half-integer quadrupolar nuclei.

2. Theory

Our MP-CPMAS experiment is based on the conventional CPMAS sequence where one replaces the CW spin-lock pulse on the quadrupolar nucleus by low RF rotor-synchronized multiple pulses using the same phase (Oy) shifted by 90° relative to the initial pulse (Ox). Here, low RF means that one wants to manipulate only the central transition (CT), which thus behaves as a fictitious spin $\frac{1}{2}$. Indeed, a low RF-field in the order of a few kHz does not affect satellite transitions and avoids uncontrollable transfer to satellite coherences [11,12,16]. We will call these pulses CT-selective. Fig. 1 shows the sequence when transferring magnetization from the quadrupolar nucleus. We will also show results for the opposite transfer (spin 1/2 to quadrupolar nucleus) in Fig. 9.

During the multiple CT-selective train pulses the first-order anisotropic interactions are averaged by MAS over full rotor periods and rotary resonance conditions are avoided, while the series of rotor-synchronized RF pulses acts as a spin-lock. Indeed, the pulses make the magnetization rotate around the "spin-lock" axis keeping it close to it

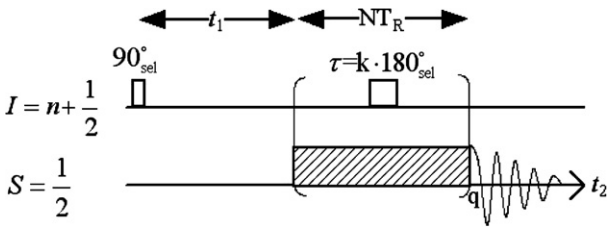

Fig. 1. Pulse-sequence for the acquisition of MP-CPMAS 2D HETCOR spectra, starting from the quadrupolar nucleus (the subscript sel stands for CT selective). Phases follow the conventional CPMAS sequence.

as long as dephasings due to offsets are not too strong. Of course, this is true only as long as the non-refocusable transverse (T_2') relaxation time (instead of $T_{1\rho}$ in CW-CPMAS) is long enough to avoid signal decay during the spin-lock period.

In the following, the observed nucleus will always be denoted S and the non-observed I. In the standard CW-CPMAS method performed under fast MAS with weak CT-selective irradiation of the quadrupolar I nucleus, the two effective RF-fields (ν_{1S}, ν_{1I}^{eff}) are related each other by the extended Hartmann–Hahn conditions [3,11,12,16]:

$$\nu_{1S} = \varepsilon\nu_{1I}^{eff} \pm j\nu_R \tag{1}$$

with $j = 0$, **1**, **2**, 3,... and $\varepsilon = \pm 1$. In the case of very fast MAS only the $j = 1$ and 2 conditions are efficient. ε corresponds to flip-flop (+1) or flop-flop (−1) terms leading to CP transfer of opposite signs.

For quadrupolar CT-selective RF-field we have $\nu_{1I}^{eff} = (I + 1/2)\nu_{1I}$, where ν_{1I} is the field measured in the absence of the quadrupolar coupling, for example on a liquid.

Following the treatment in S-AMCP [9,10], in MP-CPMAS one must consider the averaged effective field ($\bar{\nu}_{1I}^{eff}$) instead of ν_{1I}^{eff}. For one pulse every N rotor periods (NT_R) one has:

$$\bar{\nu}_{1I}^{eff} = \nu_{1I}^{eff}\tau/NT_R = \nu_{1I}^{eff}k\tau_{\pi sel}\nu_R/N = k\nu_R/2N \tag{2}$$

where the pulse-length (τ) has been scaled by the factor k with respect to that of a CT-selective π pulse ($\tau_{\pi sel}$) using the same effective RF-field. As example, for a spin 5/2 nucleus, if the RF pulse specifications are: $\tau = 8.333$ μs and $\nu_{1I} = 10$ kHz ($\tau_{\pi sel} = 50/3 = 16.667$ μs), then $k = 0.5$. Let us introduce the duty-cycle parameter p equal to the ratio between the pulse-length and the rotor period:

$$p = \tau/T_R = k\tau_{\pi sel}/T_R = 0.5k\nu_R/\nu_{1I}^{eff} \tag{3}$$

Eq. (2) assumes that one pulse fits into N rotor periods, that is:

$$k\tau_{\pi sel} < N/\nu_R \text{ or } k/2N < (I + 1/2)\nu_{1I}/\nu_R \text{ or } p < N \tag{4}$$

By replacing the I RF-field by its time average, one can rewrite Eq. (1) as:

$$\nu_{1S} = (\varepsilon k/2N \pm j)\nu_R, \quad (j = 0, \mathbf{1}, \mathbf{2}, 3, \ldots) \tag{5}$$

As already discussed before, for quadrupolar nuclei one must use weak RF fields. One may also wish to spin very fast in order to enhance proton resolution or to drive the sidebands out of the spectral range or to get sufficiently large indirect spectral width in rotor-synchronized 2D experiments. Therefore, the factor $k/2N$ is usually smaller than 1, and hence Eq. (5) can be simplified as:

$$\nu_{1S} = (\varepsilon k/2N + j)\nu_R, \quad (j = 0, \mathbf{1}, \mathbf{2}, 3, \ldots) \tag{6}$$

In the case of very fast MAS mainly the $j = 1$ and 2 conditions are efficient, which gives rise to four main resonances, with ν_{1S} frequencies pair-wise symmetrical with respect to ν_R and $2\nu_R$: two with flip-flop and two with flop-flop transfers ($\varepsilon = +1$ or -1, respectively). When the pulse-length is short, as in the $^1H \rightarrow {}^{13}C$ experiment previously described ($k = 0.19$) [18], two matching fields are close to ν_R and the two others to $2\nu_R$.

A partial signal cancellation occurs at $\nu_{1S} = 1.5\nu_R$ when the condition $k = N$ is fulfilled on the quadrupolar channel, e.g. one CT-selective π pulse every rotor period. This partial cancellation is related to coinciding matching conditions of flip-flop ($\varepsilon = +1$, $j = 1$) and flop-flop ($\varepsilon = -1$, $j = 2$) transfers, which are of opposite signs.

3. Experimental parameters

In preparation for the experiments, simulations were run on SIMPSON. [19] The system used for the simulations is a ^{27}Al nucleus ($C_Q = 3$ MHz, $\eta_Q = 0$) coupled to ^{31}P with a dipolar coupling of 400 Hz aligned with the electric field gradient tensor. Powder averaging was performed using 168 crystallites following the REPULSION algorithm [20]. RF-fields, spinning speed and static field are given in figure captions.

The experiments were performed on a wide bore 9.4 T and narrow bore 18.8 T Bruker Avance-II spectrometers equipped with triple resonance 3.2 mm MAS probes. We have tested the MP-CPMAS experiments on four different samples: $AlPO_4$-berlinite, $AlPO_4$-VPI5, $AlPO_4$-14, and $Na_7(AlP_2O_7)_4PO_4$.

The structure of berlinite $AlPO_4$ (space group $P3_121$) involves only one Al and one P crystallographic sites [21]. Aluminum and phosphorus atoms occupy tetrahedrally coordinated positions, Al–$(OP)_4$ and P–$(OAl)_4$, cross-linked by two different bridging oxygen atoms, O_1 and O_2. This leads to a single gaussian line for the ^{31}P MAS NMR spectrum and a single second-order quadrupolar line-shape for the ^{27}Al MAS spectrum ($C_Q = 4.07$ MHz, and $\eta_Q = 0.34$) [22].

Microporous hydrated aluminophosphate $AlPO_4$-VPI5 contains three equally populated sites for Al and P, which are coordinated with each other through one bridging oxygen [23]. Under MAS, the ^{31}P resonances are well resolved, but only two ^{27}Al peaks are observable at 9.4 T. The resonance which is labeled Al_1 represents a site between the fused four-membered rings. Two water molecules complete an octahedral coordination sphere for Al_1 and render inequivalent the tetrahedrally coordinated Al_2 and Al_3 sites, as well as the phosphorus sites P_2 and P_3 in the six-membered rings. The specific connectivities between various nuclei are as follows: Al_1 ($2P_1$, P_2, P_3), Al_2 (P_1, $2P_2$, P_3), and Al_3 (P_1, P_2, $2P_3$). The quadrupolar coupling constants C_Q for the aluminum sites are 3.95 MHz (Al_1), 1.3 MHz (Al_2), and 2.8 MHz (Al_3) [24,25].

We have also tested our sequences on a powder sample of $AlPO_4$-14, templated using isopropylamine. Its structure consists of 4-, 6-, and 8-rings pores. Its space group is $P\bar{1}$ with an inversion center. [26] The unit cell composition corresponds to $Al_8P_8O_{32}(OH)_2^-$ for the framework, plus two protonated isopropylamine $(C_3H_{10}N)^+$ ions and two water molecules [26] that undergo motions on the microsecond timescale in the 8-ring channels [27]. This AFN-type material forms a 3D channel system, made of alternating AlO_x ($x = 4$, 5, 6) and PO_4 polyhedrons, with 8-ring pores containing four different P and four different Al sites. The quadrupolar coupling constants C_Q and asymmetry parameters η_Q of Al_{1-4} are equal to 5.58, 4.08, 1.74, and 2.57 MHz and 0.97, 0.82, 0.63, and 0.7, respectively [28,29].

As for the sample of $Na_7(AlP_2O_7)_4PO_4$, there are one aluminum species, three phosphorus species and three sodium species [15,30]. The phosphate network is made of one $(P_2O_7)^{4-}$ unit where the two Q_1 phosphorous sites are close to all three Na sites and one isolated $(PO_4)^{3-}$ unit where the Q_0 phosphorous site is close to only two Na sites.

4. Results

4.1. Synchronization

First we have verified experimentally on $AlPO_4$-berlinite that the rotor-synchronization of the pulses is mandatory (Fig. 2). It is important to note that, in contrast to CW-

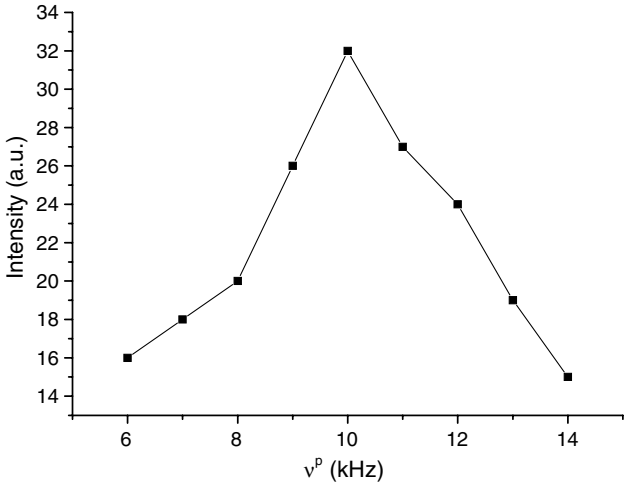

Fig. 2. ^{31}P signal observed on the $^{27}Al \rightarrow {}^{31}P$ MP-CPMAS spectrum of $AlPO_4$-berlinite ($t_1 = 0$), versus the repeat frequency of the pulses ν^P, which are applied to the aluminum channel. $B_0 = 9.4$ T, $\nu_R = 10$ kHz, $k = N = 1$, $\nu_{1Al} = 8$ kHz. ν_{1P} is optimized after every change of the frequency. The signal is maximal when rotor synchronization is achieved: $\nu^P = \nu_R$.

CPMAS [16], for MP-CPMAS of quadrupolar nuclei we have never observed any dip in the matching curve. The reason for this is that the RF-sequence applied to the quadrupolar nucleus consists of short selective pulses and thus the anti-level crossing and rotary resonance effects encountered with CW-CPMAS are avoided. This is very important when optimizing the RF-conditions on an insensitive sample. The CW RF-field applied to the spin-1/2 nucleus on the other hand is easy to optimize as its value is known in advance from Eq. (6).

4.2. Matching curves

In Fig. 3 we have simulated the absolute value of the signal versus ν_{1S}. One can see that Eq. (6) is fulfilled. For example, for $k = 0.5$ the best matching field is achieved for 7.5 kHz ($\varepsilon = -1$, $j = 1$), 12.5 kHz ($\varepsilon = +1$, $j = 1$), 17.5 kHz ($\varepsilon = 1$, $j = 2$) and 22.5 kHz ($\varepsilon = +1$, $j = 2$). For very short pulse-lengths ($0 < k < 0.5$) the transfer efficiency remains poor; but when k increases, the spin-locking of the I nucleus becomes more efficient. It reaches a maximum for $0.5 \leqslant k \leqslant 0.9$, and then decreases for k equal to 1, for which only three matching conditions ($\nu_{1S}/\nu_R = 0.5, 1.5, 2.5$) are observable. In the latter case ($k = 1$), resonances are much less efficient than those observed for $0.5 \leqslant k \leqslant 0.9$. This decrease of the signal is related to a partial signal cancellation due to overlap of flip-flop ($\varepsilon = -1$) and flop-flop ($\varepsilon = -1$) transfers, which are of opposite signs. As an example, the resonance observed at $\nu_{1S} = 15$ kHz, results from an overlap of flip-flops with $j = 1$, and flop-flops with $j = 2$. When the CP transfer is made to, not from, the quadrupolar nucleus the matching curves are exactly the same, except that ν_{1S} is exchanged with ν_{1I}.

4.3. CT-selective pulses

With moderate or large quadrupole interactions, only the central transition (CT) is observable on powder samples, and most of the time ($C_Q \gg 100$ kHz) soft CT-selective RF pulses must be used in order to control the evolution of the density matrix during the dipolar transfer. Indeed, when this is not the case the coherences will spread all over the density matrix after a few pulses, instead of remaining localized within the $+1/2 \leftrightarrow -1/2$ one-quantum coherences, as it is the case when using weak RF-fields. Simulations have shown that for $\nu_{1I} \geqslant 20$ kHz, most of the time ($C_Q \gg 100$ kHz), the signal decreases considerably in the same way as for CW-CPMAS [16]. This fact has been experimentally confirmed on our test sample, $AlPO_4$-berlinite ($C_Q = 4.07$ MHz, $\eta_Q = 0.34$) [22]. Indeed, in Fig. 4, one can observe a decrease in efficiency of approximately a factor of 2 when increasing the RF-field from 5 to 20 kHz.

4.4. Non-uniform CT excitation

We have also checked the effect of non-uniform CT excitation by RF pulses. Fig. 5 shows a simulation made for two field-strengths, $B_0 = 9.4$ T (a) and 18.8 T (b). For each, we have simulated for several C_Q the efficiencies that can be

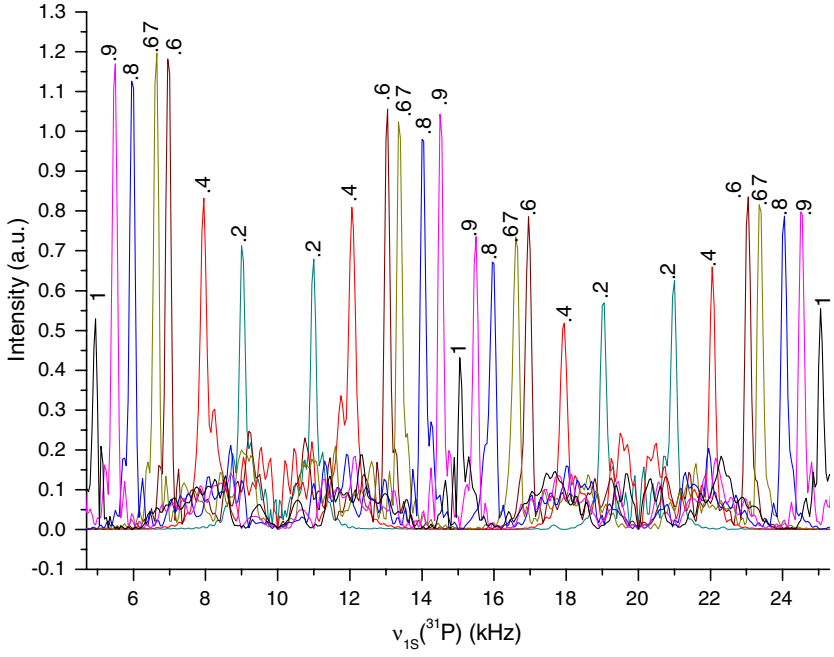

Fig. 3. $^{27}Al \rightarrow {}^{31}P$ MP-CPMAS HETCOR absolute-value of the signal ($t_1 = 0$) versus ν_{1S}, simulated with SIMPSON. $B_0 = 9.4$ T, on-resonance irradiation, ν_{1I} (^{27}Al) $= \nu_R = 10$ kHz, $C_Q = 3$ MHz, $\eta_Q = 0$, $D_{IS} = 400$ Hz aligned with the largest component of the aluminum electric-field gradient tensor, one rotor-synchronized pulse every rotor period ($N = 1$). The k value is indicated for each matching condition. The duty-cycle parameter is equal to $p = 0.033$, 0.067, 0.100, 0.133, 0.167 for $k = 0.2$, 0.4, 0.6, 0.8, 1.0, respectively.

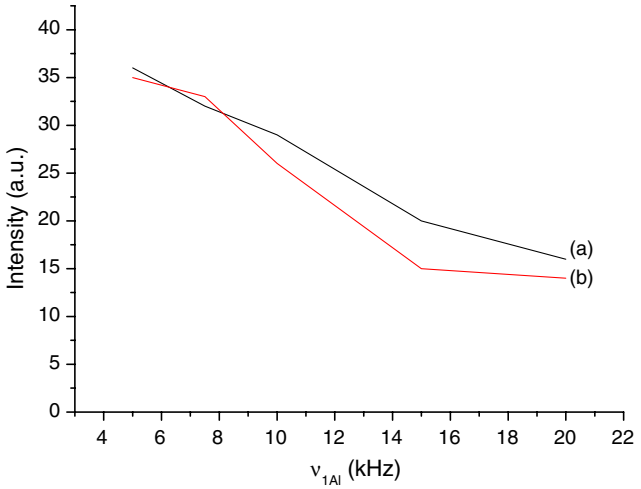

Fig. 4. ^{31}P experimental signal intensity versus the ν_{1Al} RF-field amplitude, observed on the $^{27}Al \rightarrow {}^{31}P$ MP-CPMAS spectrum of $AlPO_4$-berlinite ($t_1 = 0$), $k = N = 1$, on-resonance irradiations. (a) $B_0 = 9.4$ T, $\nu_{1P} = 5$ kHz, $\nu_R = 10$ kHz. (b) $B_0 = 18.8$ T, $\nu_{1P} = 10$ kHz, $\nu_R = 20$ kHz. The duty-cycle parameter p varies from 0.333 ($\nu_{1Al} = 5$ kHz) to 0.083 ($\nu_{1Al} = 20$ kHz), or from 0.666 ($\nu_{1Al} = 5$ kHz) to 0.167 ($\nu_{1Al} = 20$ kHz), according to B_0 is equal to 9.4 or 18.8 T, respectively.

obtained with different flip angles 180^o_{sel} ($k = 1$, $\nu_{1S} = 0.5\nu_R$), 120^o_{sel} ($k = 2/3$, $\nu_{1S} = 2\nu_R/3$), and 90^o_{sel} ($k = 0.5$, $\nu_{1S} = 0.75\nu_R$). The curves corresponding to 180^o_{sel} pulses are only shown to remind that this case, which is subject to a partial cancelling of the flip-flop and flop-flop signals, is always the least efficient. For increasing quadrupole interactions the behavior of the other curves is identical: for weak C_Q the signal first increases, then it follows a plateau and finally it decreases for large C_Q. For small quadrupole interactions (c.a. $C_Q \leqslant 2$–3 MHz), the RF excitation is too strong and hence not fully CT-selective and the evolution of the density matrix is not perfectly controlled. Taking into account the RF and quadrupolar specifications introduced in the simulations, the total static CT line-width is $\Delta = 3 \cdot 10^{-10} C_Q^2$ ($\Delta = 1.2$ kHz to 19.2 kHz for $C_Q = 2$ MHz to 8 MHz, respectively) at $B_0 = 9.4$ T and $\Delta = 1.5 \cdot 10^{-10} C_Q^2$ ($\Delta = 600$ Hz to 9.6 kHz for $C_Q = 2$ MHz to 8 MHz, respectively) at 18.8 T, respectively. For large C_Q values the RF-field ν_{1I} becomes insufficient to irradiate uniformly the whole CT line-width and the signal decreases. This occurs if C_Q is larger than c.a. 3 MHz or 4.5–5 MHz for $B_0 = 9.4$ and 18.8 T, respectively. Fig. 5 also confirms that the CP efficiency decreases when second-order quadrupolar interaction ($\propto C_Q^2/B_0$) increases; hence higher static magnetic fields are useful when observing sites with larger C_Q. The evolution of the threefold and fourfold rotation efficiencies are very similar, however the first ones are always slightly larger than the seconds.

4.5. Pulse flip angle effect

In Fig. 6 is represented the $^{27}Al \rightarrow {}^{31}P$ signal that have been observed on $AlPO_4$-berlinite at $B_0 = 9.4$ and 18.8 T.

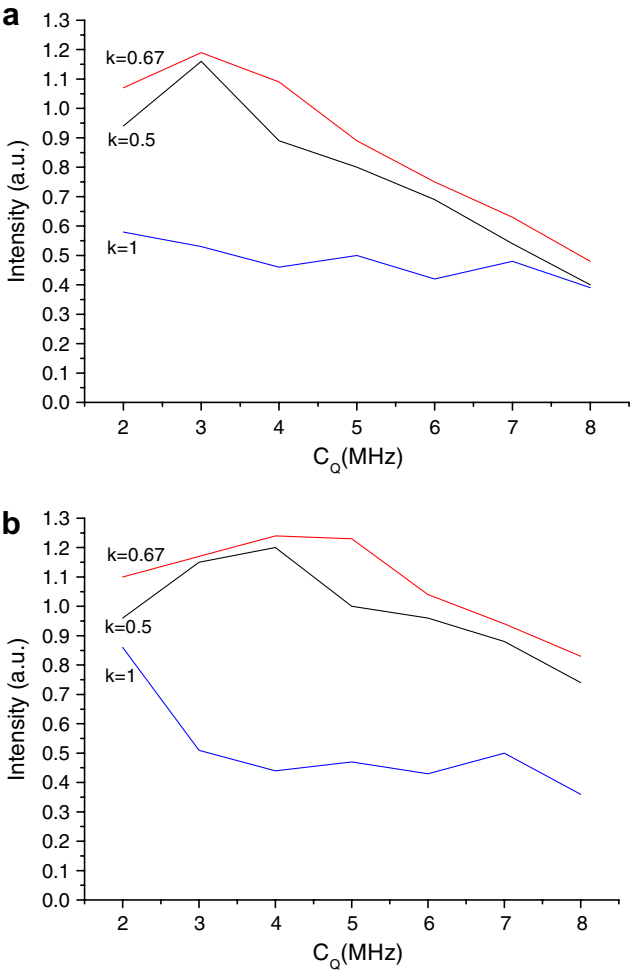

Fig. 5. $^{27}Al \rightarrow {}^{31}P$ MP-CPMAS signal ($t_1 = 0$) versus C_Q, simulated with SIMPSON. The conditions are: on-resonance irradiation, ν_{1I} (^{27}Al) = $\nu_R = 10$ kHz, $\eta_Q = 0$, $D_{IS} = 400$ Hz aligned with the largest component of the aluminum electric-field gradient tensor, one rotor-synchronized pulse every rotor period ($N = 1$), $B_0 = 9.4$ T (a), or 18.8 T (b). The three k values corresponding to the simplest r-fold rotation about Oy are indicated: $k = 1$ ($r = 2$, 180^o_{sel}), 0.67 ($r = 3, 120^o_{sel}$), and 0.5 ($r = 4, 90^o_{sel}$). The duty-cycle parameter is equal to $p = 0.167$, 0.111, and 0.083, according to k is equal to 1, 0.67, and 0.5, respectively.

The RF amplitude was fixed to $\nu_{1Al} = 7.5$ kHz, but the pulse-length τ was changed to cover a flip angle varying between 36^o_{sel} and 180^o_{sel}. For small flip angles the magnetization is not rotated fast enough to remain close to the spin-lock axis, while a flip angle of 180^o_{sel} ($k = 1$) leads to destructive overlap of flip-flop and flop-flop transfers. In between, one observes a broad maximum. Experimentally, maximum signal occurs for pulse flip angles close to 120^o_{sel} and this optimum condition leads to a larger sensitivity than the CW-CPMAS transfer.

4.6. Offsets

It is well-known that using a very weak RF-field leads to a large offset sensitivity. Thus another limitation for standard CW-CPMAS transfers involving quadrupolar

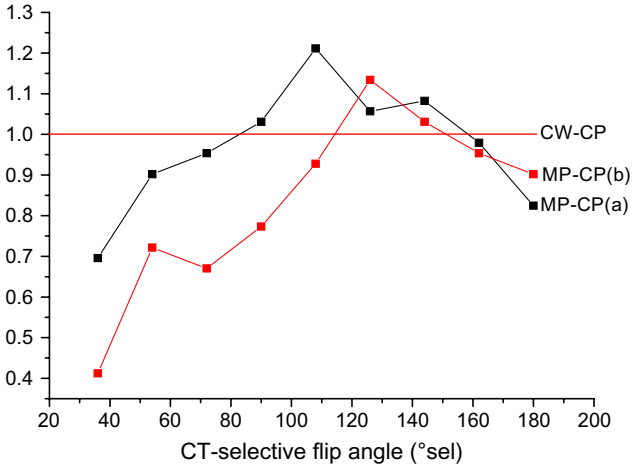

Fig. 6. ^{31}P MP-CPMAS signal ($t_1 = 0$) versus the flip angle expressed in CT-selective flip angles ($^{\circ}_{sel}$), observed on the ^{27}Al → ^{31}P spectrum of $AlPO_4$-berlinite. The parameters are $\nu_{1Al} = 7.5$ kHz, $N = 1$, ν_{1P} is optimized after the change of pulse-length. (a) $B_0 = 9.4$ T, $\nu_R = 10$ kHz. (b) $B_0 = 18.8$ T, $\nu_R = 20$ kHz. Both signals have been scaled with respect to the optimum CW-CPMAS signals observed for the same ν_R and ν_{1Al} values. The duty-cycle parameter p varies from 0.049 (40°_{sel}) to 0.222 (180°_{sel}), or from 0.098 (40°_{sel}) to 0.444 (180°_{sel}), according to B_0 is equal to 9.4 T (a) or 18.8 T (b), respectively. It is equal to 1 for CW-CPMAS.

nuclei is the attenuation due to the RF offset. Indeed, this attenuation is often very important due to the use of weak CW RF-fields during a relatively long time ($\approx 1/D_{IS}$) resulting in very narrow offset line-widths [16]. In the case of MP-CPMAS experiments, the RF is applied in a completely different way, which thus leads to a different offset sensitivity, especially on the quadrupolar channel where the multiple-pulses are applied. This can be observed in Fig. 7, where the aluminum offset effects are shown that are observed on $AlPO_4$-berlinite with standard CW-CPMAS (Fig. 7a), or with MP-CPMAS using either 180°_{sel} (Fig. 7b) or 120°_{sel} (Fig. 7c) pulses. CW-CPMAS has a quite narrow response to offset irradiation while MP-CPMAS exhibits an unusual behavior with strong inverted off-resonance signals. Thus we can imagine 2D HETCOR experiments on samples with very large chemical shift offsets in a single shot. However, some of the through-bond cross-peaks may then appear with a negative sign.

The offset sensitivity on the side of the spin-1/2 nucleus is similar to that observed in standard CW-CPMAS experiments. However, the RF-amplitude on spin-1/2 nucleus is proportional to the spinning speed (e.g. $\nu_{1S} = 2\nu_R/3$ if $k = 2/3$), and thus the offset sensitivity would be small with very fast MAS.

4.7. Very fast spinning

An important issue with modern solid-state NMR methods is how easily they can be adapted to the very fast spinning speeds (of up to 80 kHz) that have recently become available. Indeed, for reasons of resolution and sensitivity, experiments are performed at increasingly high magnetic fields, which often requires very fast MAS rates to minimize the appearance of spinning sidebands due to chemical-shift anisotropy. At these very fast speeds, the main problem encountered when manipulating quadrupolar nuclei is related to the length of the CT-selective pulses with respect to the rotor period. As an example, for a spin-3/2 nucleus with an RF-field of 10 kHz (classical value for a CT-selective irradiation: Fig. 4) the CT-selective π pulses can last up to two rotor periods for very fast spinning speeds such as $\nu_R = 80$ kHz, and thus the selective pulses must then be separated by several (N) rotor periods. We have analyzed with SIMPSON the optimum value of rotor periods (N_{opt}) versus the spinning speed, for two different RF-fields (ν_{1I}) (Table 1). For spinning speeds faster than 40 kHz, the signal is negligible for $N = 1$, it becomes maximum for a few rotor periods (N_{opt}), and then decreases to zero for very long delays. For a fixed RF-field

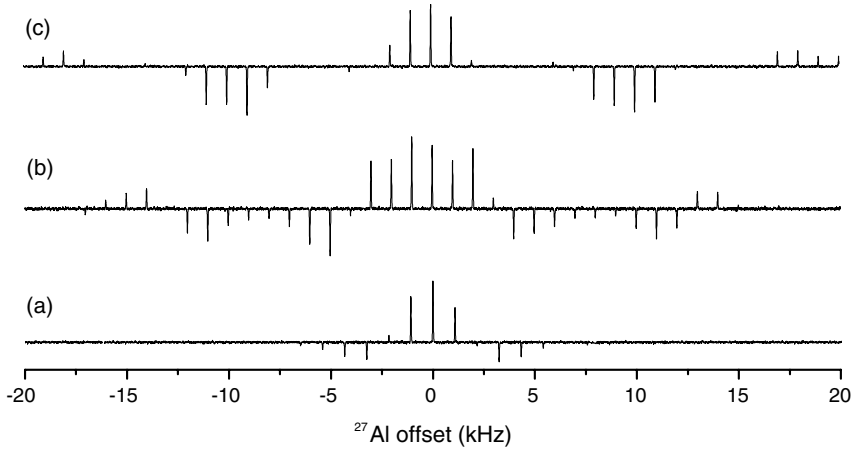

Fig. 7. ^{27}Al offset sensitivity observed on the ^{27}Al → ^{31}P spectrum of $AlPO_4$-berlinite. $\nu_R = 10$ kHz, $\nu_{1Al} = 7.5$ kHz, $B_0 = 9.4$ T, (a) CW-CPMAS, (b) MP-CPMAS with $k = 1$, (c) MP-CPMAS with $k = 0.67$. The duty-cycle parameter is equal to $p = 1$ (a), 0.222 (b), 0.148 (c), respectively.

Table 1
Optimum number of rotor periods (N_{opt}) between two consecutive pulses, and related signal, that can be observed for different spinning speeds and two ν_{1I} values

ν_{1I}	5 kHz		8 kHz	
ν_R (kHz)	N_{opt}	Signal (a.u)	N_{opt}	Signal (a.u)
10	1	1.02	1	1.15
30	3	0.98	3	0.90
50	5	0.90	5	0.88
70	7	0.64	7	0.76

$B_0 = 9.4$ T, $S = {}^{31}$P, I = ^{27}Al, pulse-length: 120^{o}_{sel} ($k = 2/3$), $C_Q = 3$ MHz, $D_{IS} = 400$ Hz aligned with the quadrupolar tensor ($\eta_Q = 0$), on-resonance irradiations.

For $\nu_{1I} = 5$ kHz and $\nu_R = 70$ kHz, the pulse lasts 1.6 rotor periods, and hence the signal decreases considerably. This effect is less important for $\nu_{1I} = 8$ kHz, where the pulse lasts only 1 rotor period.

(ν_{1I}), the optimum signal slowly decreases with increasing spinning speed except for very small ν_{1I} values.

It can be observed in Table 1 that for a given RF-field, the optimum number of rotor periods is approximately proportional to the spinning speed, thus corresponding to a constant averaged RF-field $\bar{\nu}_{1I}$. This is exactly what has been observed for $^{1}H \rightarrow {}^{13}C$ MP-CPMAS transfers: the optimum transfer was observed with approximately the same ^{1}H averaged RF-field: 4 kHz with CW-CPMAS and 5.9 kHz (280 kHz*0.35/16.667) with MP-CPMAS [18]. This constant $\bar{\nu}_{1I}$ value can be obtained in two ways: one soft pulse every N_{opt} rotor periods, or one soft pulse N_{opt} times shorter every rotor period. However, simulations and experiments have shown that the first case is slightly better because fewer pulses are used. Another explanation may be that shorter pulses do not rotate properly all crystallite magnetizations within the quadrupolar line-width, while longer pulses benefit from crystallite sweep due to the rotation. As an example, on $AlPO_4$-berlinite with $\nu_R = 20$ kHz, the experimental signal was 13% larger with one pulse of 15.4 μs ($\approx 120^{o}_{sel}$) every two rotor periods than with one pulse of 7.7 μs ($\approx 60^{o}_{sel}$) every rotor period ($\nu_{1Al} = 7.5$ kHz, $B_0 = 9.4$ T, $\nu_{1P} = 13.3$ kHz, $qN_{opt}T_R = 5$ ms).

4.8. HETCOR spectra

The $^{27}Al \rightarrow {}^{31}P$ MP-CPMAS HETCOR spectrum of $AlPO_4$-VPI5, recorded at 9.4 T, is displayed in Fig. 8. Due to much more favorable relaxation times, we started the experiments from the aluminum nuclei. The resolution along the phosphorus axis has been enhanced by introducing an aluminum decoupling pulse sequence optimized for quadrupolar nuclei [31]. It can be observed that, in agreement with the structure, all aluminum atoms are spatially close to all phosphorus atoms.

The $^{1}H \rightarrow {}^{27}Al$ HETCOR spectrum of $AlPO_4$-14 shown in Fig. 9 has been recorded also at 9.4 T. Due to its larger C_Q value, and the moderate field, cross-peaks with Al_1 spe-

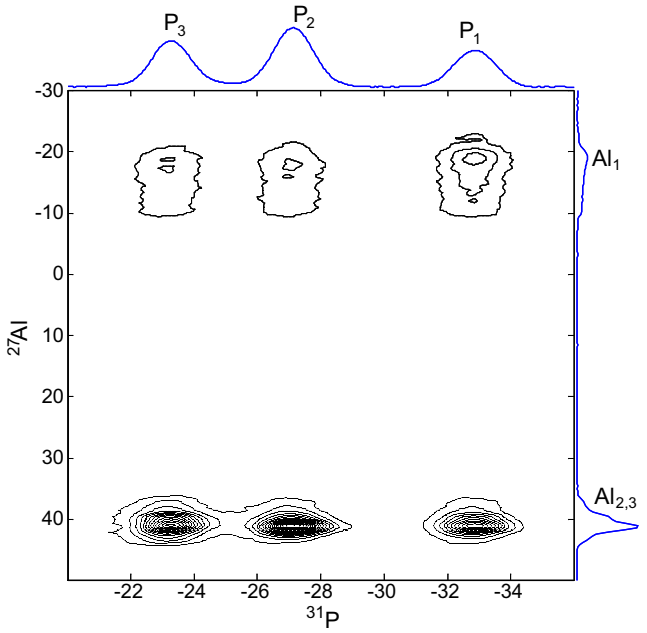

Fig. 8. $AlPO_4$ VPI5 $^{27}Al \rightarrow {}^{31}P$ MP-CPMAS HETCOR spectrum. $\nu_R = 10$ kHz, $B_0 = 9.4$ T. 320 scans per row and recycling delay of 2 s. Total experimental time = 18 h. $\nu_{1Al} = 7$ kHz, $\nu_{1P} = 14.3$ kHz, $k = 0.9$ and $N = 1$.

cies are hardly visible. The correlations observed are equivalent to those described in Fig. 3 of reference [32].

Finally, MP-CPMAS has been tested on a spin 3/2 system and on a larger magnetic field. The $^{23}Na \rightarrow {}^{31}P$ MP-CPMAS HETCOR experiment was performed at 18.8 T on $Na_7(AlP_2O_7)_4PO_4$. We can observe in Fig. 10 that the P_2 (Q_0) site is only correlating with Na_1 and Na_2 sites, which is in agreement with the structure.

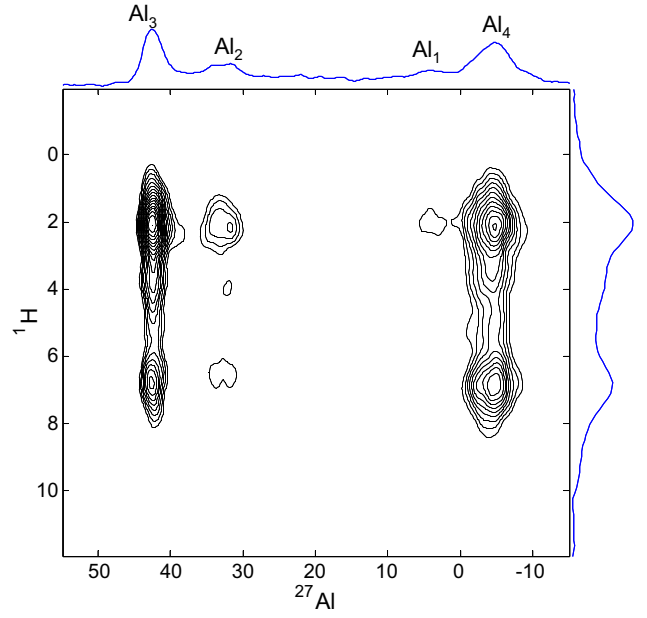

Fig. 9. $AlPO_4$-14 $^{1}H \rightarrow {}^{27}Al$ MP-CPMAS HETCOR spectrum. $\nu_R = 10$ kHz, $B_0 = 9.4$ T. 200 scans per row and recycling delay of 1 s. Total experimental time = 4.5 h. $\nu_{1Al} = 6.4$ kHz, $\nu_{1P} = 14.6$ kHz, $k = 0.9$ and $N = 1$.

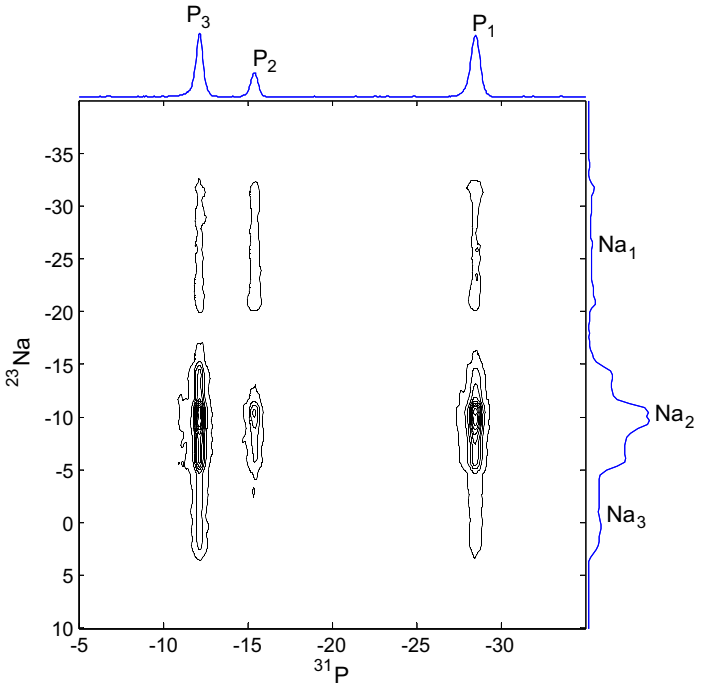

Fig. 10. $Na_7(AlP_2O_7)_4PO_4$. $^{23}Na \rightarrow {}^{31}P$ MP-CPMAS HETCOR spectrum. $\nu_R = 20$ kHz, $B_0 = 18.8$ T. 32 scans per row and recycling delay of 3 s. Total experimental time: 128 min. $\nu_{1Al} = 7.8$ kHz, $\nu_{1P} = 16.6$ kHz, $k = 0.7$ and $N = 2$.

5. Conclusion

We have shown that the continuous-wave spin-locking of quadrupolar nuclei can be replaced by rotor-synchronized multiple-pulse spin-locking. In this case, one must consider the average RF-field produced by the pulses in order to fulfill the Hartmann–Hahn matching equation. MP-CPMAS is more efficient, more robust and less sensitive to offsets on the side of the quadrupolar nucleus than standard CW-CPMAS. It is thus particularly useful for 2D HETCOR experiments. The experiment is quite broad-banded with respect to the pulse-length which must be between 0.5 and 0.9 times that of a CT selective π pulse. We find that using rotor-synchronized selective $2\pi/3$ pulses seems to be the most efficient way to perform MP-CPMAS experiments.

Acknowledgments

B.H., J.T., and J.P.A thank Region Nord/Pas de Calais, Europe (FEDER), CNRS, French Minister of Science, USTL, FR-3950, ENSCL and the Bruker company for funding. At Lille, this research was supported by the ANR contract NT05-2-41632. Authors thank one of the referees for several helpful comments.

References

[1] S.R. Hartmann, E.L. Hahn, Phys. Rev. 128 (1962) 2042.
[2] A. Pines, M.G. Gibby, J.S. Waugh, J. Chem. Phys. 56 (1972) 1176.
[3] E.O. Stejskal, J. Schaefer, J.S. Waugh, J. Magn. Reson. 28 (1977) 105.
[4] P. Caravatti, G. Bodenhausen, R.R. Ernst, Chem. Phys. Lett. 89 (1982) 363–367.
[5] D.P. Burum, A. Bielecki, J. Magn. Reson. 94 (1991) 645–652.
[6] G. Metz, X.L. Wu, S.O. Smith, Ramped-amplitude cross polarization in magic-angle-spinning NMR, J. Magn. Reson., Ser. A 110 (1994) 219–227.
[7] X. Wu, K.W. Zilm, Cross polarization with high-speed magic-angle spinning, J. Magn. Reson., Ser. A 104 (1993) 154–165.
[8] S. Hediger, B.H. Meier, R.R. Ernst, Cross polarization under fast magic angle sample spinning using amplitude-modulated spin-lock sequences, Chem. Phys. Lett 213 (1993) 627–635.
[9] S. Hediger, B.H. Meier, R.R. Ernst, Rotor-synchronized amplitude-modulated nuclear magnetic resonance spin-lock sequences for improved cross polarization under fast magic angle sample spinning, J. Chem. Phys. 102 (1995) 4000.
[10] J. Raya, J. Hirschinger, Application of rotor-synchronized amplitude-modulated cross-polarization in a ^{13}C–^{1}H spin pair under fast MAS, J. Magn. Reson 133 (1998) 341–351.
[11] A.J. Vega, MAS NMR spin-locking of half-integer quadrupolar nuclei, J. Magn. Reson. 96 (1992) 50–68.
[12] A.J. Vega, CPMAS of quadrupolar $S = 3/2$ nuclei, Solid State NMR 1 (1992) 17–32.
[13] M.A. Eastman, Examples of Hartmann–Hahn match conditions for CW-CPMAS between two half-integer quadrupolar nuclei, J. Magn. Reson. 139 (1999) 98–108.
[14] J.C.C. Chan, High-resolution hetero-nuclear correlation between quadrupolar nuclei, J. Magn. Reson. 140 (1999) 487–490.
[15] G. Tricot, L. Delevoye, G. Palavit, L. Montagne, Phase identification and quantification in a devitrified glass using homo- and heteronuclear solid-state NMR, Chem. Commun. 42 (2005) 5289–5291.
[16] J.P. Amoureux, M. Pruski, Theoretical and experimental assessment of single- and multiple-quantum cross-polarization in solid-state NMR, Mol. Phys. 100 (2002) 1595–1613.
[17] T.G. Oas, R.G. Griffin, M.H. Levitt, Rotary resonance recoupling of dipolar interactions in solid-state nuclear magnetic resonance spectroscopy, J. Chem. Phys 89 (1988) 692–695.

[18] S. Hafner, A. Palmer, M. Cormos, Ultra-Fast Magic-Angle Spinning, Talk at 13th National Indian NMR Meeting, February 5–8. 2007, Pune, India.
[19] M. Baks, J.T. Rasmussen, N.C. Nielsen, SIMPSON: a general simulation program for solid-state NMR spectroscopy, J. Magn. Reson. 147 (2000) 296–330.
[20] M. Baks, N.C. Nielsen, REPULSION: a novel approach to efficient powder averaging in solid-state NMR, J. Magn. Reson. 125 (1997) 132–139.
[21] A. Goiffon, J.C. Jumas, M.M. Aurin, E. Philippot, J. Solid State Chem. 61 (1986) 384–396.
[22] C. Huguenard, F. Taulelle, B. Knott, Z. Gan, Optimizing STMAS, J. Magn. Reson. 156 (2002) 131–137.
[23] L. B McCusker, Ch. Baerlocher, E. Jahn, M. Bülow, The triple helix inside the large-pore aluminophosphate molecular sieve VPI-5, Zeolites 11 (1991) 308–313.
[24] J. Rocha, W. Kolodziejski, H. He, J. Klinowski, Solid-state NMR studies of hydrated porous aluminophosphate VPI-5, J. Am. Chem. Soc. 114 (1992) 4884–4888.
[25] C. Fernandez, C.M. Morais, J. Rocha, M. Pruski, High-resolution hetero-nuclear correlation spectra between ^{31}P and ^{27}Al in microporous aluminophosphates, Solid State Nucl. Magn. Reson. 21 (2002) 61–70.
[26] R.W. Broach, S.T. Wilson, R.M. Kirchner, Corrected crystallographic tables and figure for as synthesized $AlPO_4$-14, Micropor. Mesopor. Mater. 57 (2003) 211–214.
[27] S. Antonijevic, S.E. Ashbrook, S. Biedasek, R.I. Walton, S. Wimperis, H. Yang, Dynamics on the microsecond timescale in microporous aluminophosphate $AlPO_4$-14 as evidenced by ^{27}Al MQMAS and STMAS NMR spectroscopy, J. Am. Chem. Soc. 128 (2006) 8054–8062.
[28] C. Fernandez, J.P. Amoureux, J.M. Chezeau, L. Delmotte, H. Kessler, ^{27}Al MAS NMR characterization of $AlPO_4$-14. Enhanced resolution and information by MQMAS, Micropor. Mater. 6 (1996) 331–340.
[29] C.A. Fyfe, H.M.z. Altenschildesche, K. Wong-Moon, H. Grondey, J.M. Chezeau, 1D and 2D solid state NMR investigations of the framework structure of As-synthesized $AlPO_4$-14, Solid State NMR 9 (1997) 97–106.
[30] M. de la Rochère, A. Kahn, F. d'Yvoire, E. Bretey, Crystal structure and cation transport properties of the ortho-diphosphates $Na_7(MP_2O_7)_4PO_4$ (M = Al, Cr, Fe), Mater. Res. Bull. 20 (1985) 27–34.
[31] L. Delevoye, J. Trebosc, Z.H. Gan, L. Montagne, J.P. Amoureux, Resolution enhancement using a new multiple-pulse decoupling sequence for quadrupolar nuclei, J. Magn. Reson. 186 (2007) 94–99.
[32] J. Trebosc, B. Hu, J.P. Amoureux, Z. Gan, Through-space R^3-HETCOR experiments between spin-1/2 and half-integer quadrupolar nuclei in solid-state NMR, J. Magn. Reson. 186 (2007) 220–227.